Acta Materialia 215 (2021) 117083

Contents lists available at ScienceDirect

Acta Materialia

journal homepage: www.elsevier.com/locate/actamat

Full length article

Extraordinarily strong magneto-responsiveness in phase-separated $LaFe_2Si$

Arjun K. Pathak[a,*], Yaroslav Mudryk[b], Nikolai A. Zarkevich[b,c], Dominic H. Ryan[d], Duane D. Johnson[b,e], Vitalij K. Pecharsky[b,e]

[a] Department of Physics, SUNY Buffalo State, Buffalo, NY 14222 United States
[b] Ames Laboratory, U. S. Department of Energy, Ames, Iowa 50011-2416, United States
[c] NASA Ames Research Center, Moffett Field, California 94035, United States
[d] Physics Department and Centre for the Physics of Materials, McGill University, 3600 University Street, Montreal, Quebec, H3A 2T8, Canada
[e] Department of Materials Science and Engineering, Iowa State University, Ames, Iowa 50011-1096, United States

ARTICLE INFO

Article history:
Received 29 January 2021
Revised 10 May 2021
Accepted 10 June 2021
Available online 15 June 2021

Keywords:
Magnetocaloric
Intermetallics
Magnetoresistance
Phase transitions

ABSTRACT

Materials responding vigorously to minor variations of external stimuli with negligible hysteresis could revolutionize many of the energy technologies, including refrigeration, actuation, and sensing. We report a combined experimental and theoretical study of a two-phase composite, naturally formed at the $LaFe_2Si$ stoichiometry, which exhibits a nearly anhysteretic, two-step first-order ferromagnetic-to-paramagnetic phase transformation with enhanced sensitivity to an external magnetic field. Other unusual properties include a large plateau-like positive magnetoresistance, magnetic-field-induced temperature and entropy changes occurring over a wide temperature range, and a Griffiths-like phase associated with short-range ferromagnetic clustering in the paramagnetic state. The heat capacity, magnetization, Mössbauer spectroscopy, and electrical resistivity, all exhibit characteristic, unusually sharp, first-order discontinuities even in magnetic fields as high as 100 kOe. We expect that similar phenomena could be designed in other mixed-phase systems, leading to novel functionalities, such as giant caloric effects in many yet undiscovered or/and underperforming intermetallic compounds.

1. Introduction

Energy-efficient, environmentally-benign magnetocaloric cooling, or, more generally, magnetocaloric heat pumping, has become a lively subject of research following discoveries of the giant magnetocaloric effect in $Gd_5Si_{4-x}Ge_x$ [1] and a few other families of materials [2–8], and laboratory demonstration of a heat pump, where the giant magnetocaloric effect of $LaFe_{13-x}Si_xH_y$ was put to use [9]. Giant magnetocaloric effects arise from first-order magnetic phase transformations (FOMPTs), hence significant hysteresis and poor thermal transport remain two materials-related basic science challenges that impede the transitioning of the magnetocaloric cooling technologies to market [10,11]. Preserving giant magnetocaloric effects while reducing hysteresis to eliminate irreversibility has emerged as a major research area in rare-earth (R) metal-based $LaT_{13-x}Si_xH_y$, where T = Fe mixed with late 3*d*-metals and R_5X_4, where X = group 14 element, and in transition metal-based Ni_2TX and MnTX, where T = {Mn, Fe, Co, Ni, Cu} and X = {Al, Si, Ge, Sn, Ti} [12–18]. Considering the natural abundance of the constituting elements, $LaFe_{13-x}Si_x$-derived compounds are among the most promising materials for energy applications [9,19-22]. They are, however, extremely brittle and mechanically friable, showing rather low thermal conductivities and measurable irreversibilities, which thus far could not be completely eliminated.

Intermetallic compounds with general stoichiometry $LaFe_{13-x}Si_x$ crystallize in a face-centered cubic $NaZn_{13}$-type structure (space group $Fm\bar{3}c$) with eight formula units per cell. The binary $LaFe_{13}$ compound is unstable due to a positive heat of formation relative to La and Fe elemental solids. However, this structure can be stabilized by adding a third element, for example, Si in $LaFe_{13-x}Si_x$ when $x \geq 1.2$. In a 112-atom, face-centered cubic cell of a hypothetical $LaFe_{13}$, there are 8 La atoms located in 8a ($^1/_4$, $^1/_4$, $^1/_4$) positions and two symmetrically independent Fe atoms: 8 Fe_1 in 8b (0, 0, 0) and 96 Fe_2 in 96i (0, y, z) [23]. Neutron powder diffraction data suggest that the Si atoms in $LaFe_{11.4}Si_{1.6}$ nearly randomly occupy both 8b and 96i sites [23]. The Fe_1-Fe_2 distance plays an essential role in determining the strength of magnetic exchange interactions and, therefore, it affects the Curie temperature, T_C, of $LaFe_{13-x}Si_x$ [23,24].

* Corresponding author.
E-mail address: pathakak@buffalostate.edu (A.K. Pathak).

https://doi.org/10.1016/j.actamat.2021.117083
1359-6454/

As reported, $LaFe_{13-x}Si_x$ compounds with low Si content undergo magneto-volume, itinerant-electron metamagnetic (IEM) FOMPTs between ferromagnetic (FM) and paramagnetic (PM) states. These phase transformations can be induced by temperature, external magnetic field, or both [25]. Defined as the minimum of the first derivative of magnetization with respect to temperature, T_C increases with the increasing magnetic field, and it is also influenced by stress/strain [26]. The Curie temperature depends on the composition, x, rising from $T_C \approx 175$ K for $x = 1.17$ to $T_C \approx 208$ K when $x = 1.6$ [27]. Increasing x further converts this fundamentally and practically interesting FOMPT into a conventional second-order ferromagnetic-paramagnetic phase transformation [27]. In general, properties of itinerant electron metamagnets are susceptible to, and can be rationalized and controlled by, varying 3*d* electronic density of states (DOS) at the Fermi energy (E_F) [28]. Thus, substituting T = V, Cr, Ni, Cu into $La(Fe_{1-y}T_y)_{11.4}Si_{1.6}$ is both expected and known to strongly influence the *d*-electron concentration and, hence, magnetic, magnetocaloric, and magnetoelastic properties of the $LaFe_{13-x}Si_x$ parent [29].

In addition to manipulating chemistry, substantial efforts have been devoted to tailoring mechanical, thermal, and magnetocaloric properties of $LaFe_{13-x}Si_x$ by creating metal-metal composites through pressing and sintering its powders mixed with powders of other constituents. For example, samples prepared by spark-plasma sintering after adding 5% of LaAl, which promotes the formation of the $LaFe_{13-x}Si_x$ phase, show significant improvements in their magnetic properties [30]. In another example, Wang *et al.* [31] reported $LaFe_{13-x}Si_xH_y$/In composites prepared with different concentrations of indium by hot-pressing, which improves mechanical properties and thermal conductivity.

Another way to create a nearly ideal metal-metal composite is to make use of phases naturally developing in off-stoichiometric alloys. Considering that $LaFe_{13-x}Si_x$ is the phase of interest, it is important to examine how other phases present in the La-Fe-Si system coupled via the cleanest possible interfaces in two- or three-phase alloys affect the functionality of such composites. The nearly equiatomic LaFeSi compound (its homogeneity range at 873 K extends from $LaFe_{0.95}Si_{1.05}$ to $LaFe_{1.13}Si_{0.87}$ [32]) and $Fe_{1-\delta}Si_\delta$ solid solution always form in as-cast stoichiometric $LaFe_{13-x}Si_x$ alloys as the two primary solidification phases [33]. LaFeSi and $Fe_{1-\delta}Si_\delta$ must be reacted in the solid-state during post-solidification anneals to yield $LaFe_{13-x}Si_x$ [34]. The resulting annealed alloys nearly always contain some $Fe_{1-\delta}Si_\delta$, which is a soft ferromagnet with T_C far above that of $LaFe_{13-x}Si_x$, but LaFeSi is usually completely consumed upon heat treatment. Large (10-15 wt. %) concentrations of residual $Fe_{1-\delta}Si_\delta$ improve mechanical stability but this phase also adds substantial ferromagnetic background and, for example, magnetocaloric properties of two-phase $LaFe_{13-x}Si_x + Fe_{1-\delta}Si_\delta$ alloys always suffer [29].

The LaFeSi intermetallic is drastically different from both $LaFe_{13-x}Si_x$ and $Fe_{1-\delta}Si_\delta$: the nearly equatomic ternary compound is a Pauli paramagnet with no known crystallographic phase changes beyond conventional thermal expansion. So, the question arises whether LaFeSi intimately coupled with $LaFe_{13-x}Si_x$ will affect magnetism and magnetothermal behavior of such a natural composite? And, if yes, then how? Phase relationships [32] in the ternary La-Fe-Si system indicate that, for example, a rather simple $LaFe_2Si$ composition falls into a two-phase equilibrium region between $LaFe_{13-x}Si_x$ with x close to 2.2 and nearly equiatomic $LaFe_{1.1}Si_{0.9}$. The $LaFe_2Si$ stoichiometry ensures that there is a large amount of the $LaFe_{1.1}Si_{0.9}$ phase (*ca* 70 % at 873 K, according to the lever rule) to make a difference – the basic properties of nearly phase pure $LaFe_{13-x}Si_x$ are explicitly known now.

In this work, we investigate how properties of $LaFe_{13-x}Si_x$ in the two-phase system are affected by the presence of the LaFeSi matrix using temperature- and field-dependent magnetization, specific heat, powder X-ray diffraction, and electrical resistivity measurements, as well as temperature-dependent Mössbauer spectroscopy. The well-known IEM FOMPT of $LaFe_{13-x}Si_x$ splits into two related events, one of which is clearly reflected as anomalies of all measured properties, while the second transformation remains hidden in bulk magnetization and electrical resistivity data. Further, the giant magnetocaloric effect is observed over a much broader temperature range, and the thermal hysteresis is much lower when compared to those in the well-studied conventional $LaFe_{13-x}Si_x$, commonly in the presence of 5-10 % of $Fe_{1-\delta}Si_\delta$. These results confirm that the $LaFe_2Si$ alloy is indeed a naturally formed metal-metal composite containing magnetically active $LaFe_{13-x}Si_x$ and magnetically inactive LaFeSi matrix rather than a simple non-interacting two-phase mixture thereof.

2. Experimental techniques

Elemental La with 99.98+ wt.% purity with respect to all other elements in the periodic table was obtained from the Materials Preparation Center of the Ames Laboratory. At least 99.99% pure Fe and Si were purchased from Alfa Aesar Inc. A 10 *g* alloy with a nominal composition of $LaFe_2Si$ was prepared from the elements by arc melting in an argon atmosphere. First, Fe and Si were melted together and re-melted three times, followed by adding the La metal and re-melting the alloy three more times; the alloy button was flipped upside down after each re-melting. The total weight loss was 0.08 wt.%. The arc-melted button was then drop-cast into a ~1 cm diameter chilled copper mold to reduce grain sizes and achieve homogeneous solidification microstructure throughout the ingot. The drop-cast alloy was further annealed at 1323 K for two weeks in a quartz tube sealed under vacuum, followed by cooling with the furnace to room temperature after shutting down the power.

The crystal structure was determined by powder x-ray diffraction (XRD) between room temperature and 15 K in zero and applied magnetic fields up to 35 kOe using the Rigaku rotating anode diffractometer (TTRAX system, Mo Kα radiation) equipped with a continuous flow cryostat and a split-coil superconducting magnet [35]. The crystallographic parameters of both phases and phase concentrations were determined by Rietveld analysis using LHPM Rietica [36]. dc magnetization was measured with a superconducting quantum interference device magnetometer (MPMS-XL7, Quantum Design, Inc.) and with a vibrating sample magnetometer (PPMS, Quantum Design, Inc.) in magnetic fields up to 140 kOe. The heat capacity measurements were performed using a homemade adiabatic heat-pulse calorimeter [37] in zero and applied magnetic fields up to 100 kOe. Electrical resistivity measurements were performed in a four-contact configuration using PPMS. The microstructure and energy dispersive X-ray spectroscopy (EDX) measurements were carried out on an FEI Teneo scanning electron microscope (SEM) equipped with an Oxford Instruments Aztec EDX system. The ^{57}Fe Mössbauer spectroscopy measurements were carried out using a 50 mCi ^{57}Co**Rh** source, in constant acceleration mode, and calibrated using a standard α-Fe foil. Isomer shifts are quoted relative to α-Fe at ambient temperature. The sample was cooled in a vibration-isolated closed-cycle helium refrigerator with the sample in a helium exchange gas. The spectra were fitted to a sum of Lorentzian lines. The clear broadening of the magnetic component was modeled using a Gaussian distribution of hyperfine fields with the peak field and the Gaussian widths to the high and low sides as independent variables.

3. Computational methods

We used VASP [38,39] and KKR-CPA [40,41] codes to study $LaFe_{13-x}Si_x$ and LaFeSi phases: an all-electron Korringa-Kohn-

Rostoker (KKR) Green's function code [40] that is capable of addressing atomic and magnetic disorder within the coherent potential approximation (CPA) [41], and a pseudo-potential, plane-wave method embodied in VASP code [38,39]. In both codes, we used the same Perdew-Burke-Ernzerhof (PBE) exchange-correlation functional [42] and the same modified, second Broyden method [43] for accelerated convergence. We used $4 \times 4 \times 4$ Monkhorst-Pack k-meshes [44] for the Brillouin zone integration in the 112-atom unit cell of $LaFe_{13-x}Si_x$ (lattice constants and moments per site are reported in Table S1 in the supplementary information, SI). With Si doped on Fe sites, the structure is $NaZn_{13}$ (space group $Fm\bar{3}c$) with La at 8a sites, Fe_1 at 8b sites, and with Fe_2 at 96i sites with (0 y z) coordinates, as determined from the Rietveld refinement of the XRD data collected at 15 K (see below and Tables S2 and S3). The LaFeSi structure (with 2 atoms each) has a tetragonal unit cell (space group P4/nmm) with lattice constants (a, b, and c) and La, Fe, and Si sites specified in Tables S2 and S3, similar to that also found from calculations by the Materials Project [45].

KKR-CPA calculations [40,46] were performed using a site-centered spherical-harmonic basis (including s, p, d, and f orbital symmetries, i.e., $l_{max} = 3$) in a scalar-relativistic approximation (that is, no spin-orbit coupling) with periodic boundary corrections to account for interstitial electrons commensurate with crystal symmetry. The screened CPA was used to address the atomic charge-correlations (Friedel screening) on average in the random alloy [47]. The self-consistent charge density was obtained from the all-electron Green's function by means of a complex-energy (semi-circular) contour integration using a Gauss-Laguerre quadrature (i.e., 24-point mesh enclosing the bottom to the top of the valence states). The cores of La, Fe, and Si included 48, 18, and 10 electrons, respectively. The PM state was approximated by an uncorrelated disordered local moments (DLM), spherically distributed by 4π radians, easily handled within the KKR-CPA.

In VASP, atoms were fully relaxed until atomic forces did not exceed 0.024 eV/Å. We used 400 eV energy cutoff for the plane-wave basis, and Davidson-block iteration scheme (IALGO = 38) for the electronic energy minimization [38,39]. Spin-polarized calculations revealed the electronic structure of FM $LaFe_{13-x}Si_x$ at several values of x. At $x > 0$, four different representative supercells were considered at each fixed composition. Bader analysis [48] was performed to find a distribution of atomic charges and magnetic moments.

4. DFT results

According to the ternary phase diagram [32], the $LaFe_2Si$ composition should segregate into into LaFeSi and $LaFe_{13-x}Si_x$ phases. Density functional theory (DFT) shows that LaFeSi is non-magnetic (NM), with zero atomic moments, see Fig. 1(a). This agrees with the literature as experimentally no magnetic ordering has been detected for LaFeSi [49]. In contrast, the cubic $LaFe_{13-x}Si_x$ phase is magnetic, see Fig. 1(b,c,d). KKR-CPA calculations reveal that a structure with Fe/Si disorder on both Fe1 and Fe2 sites is slightly higher in energy than disorder only on Fe2 sites, in contrast to the interpretation from neutron diffraction, which may be altered by chemical entropy; nonetheless, results are reported for Fe2 disorder, see Table S1. We also note (our unpublished crystallographic data) that the p-block element is known to avoid the 8b site, for example in $LaNi_{11.4}Ge_{1.6}$, where Ge is found only on the 96i site, while the 8b site is fully occupied by Ni. KKR-CPA results reveal a strong dependence of atomic magnetic moments on the lattice constant. In the PM (DLM) state, magnetic moments, M_a, of Fe_1 and Fe_2 (see Table S1) increase from 0.547 and 2.163 Bohr magnetons (μ_B) at $a = 11.484$ Å to 0.844 and 2.229 μ_B at $a = 11.550$ Å; moments of Si and La remain zero. In the FM state, all atoms including Fe_1, Fe_2, Si, and La have nonzero M_a, which increase, respectively, from 1.54, 2.34, -0.178, and -0.325 μ_B at $a = 11.484$ Å to 1.61, 2.384, -0.181, and -0.336 μ_B at $a = 11.550$ Å. The CPA assumes a homogeneous occupancy of each sublattice, i.e., no atomic short-range order (SRO), and returns a configurationally-averaged value of M_a for each symmetry-distinctive species. In reality, there is a distribution of local moments. In VASP, Bader analysis in supercells returns distribution of atomic volumes and magnetic moments of Fe atoms, expected due to a varying local chemical environment caused by disorder on 8b and 96i sites. Average values are comparable to those from CPA, as expected.

In DFT, the equilibrium lattice constant in the PM state of $LaFe_{13-x}Si_x$ is smaller than that in the FM state, see Fig. 1(b) and the experimental data for $LaFe_{11.7}Si_{1.3}$ in Fig. S1, SI. Bond lengths are shorter in the paramagnetic state compared to the ferromagnetic state due to increased separation from the magnetic wave-function overlaps, and, as the atomic moments in the PM state are smaller, one should expect a volume change at FOMPT. Similarly, in FeRh, the Rh moment is zero in the antiferromagnetic (AFM) state, but not in the FM state, and the AFM volume is slightly smaller [50]. However, in systems like Pr_2In [51] the volume change at the FM-PM transition is negligible, and hysteresis is minimal.

DFT results provide a compositional dependence of the equilibrium lattice constant of $LaFe_{13-x}Si_x$, which decreases with x [27]. This dependence is expected due to a smaller effective atomic radius of Si compared to Fe. The electronic and spin densities of states depend on the composition. Sharp peaks and narrow pseudo-gaps are possible in ordered compounds, while atomic disorder smears them, see Fig. 1(a,c). A similar phenomenon happens in high-entropy alloys [52]. A change of electronic DOS at E_F affects the electronic entropy and contributes to the overall caloric effect [50].

As mentioned above, small induced atomic magnetic moments of Si and La in the FM phase of $LaFe_{13-x}Si_x$ are aligned antiparallel to those of the majority of Fe atoms. If an iron atom is effectively caged by Si [53] (e.g., an atom in the middle of the vertical edge in Fig. 1(d)), then its moment can align with Si neighbors and become antiparallel to that of the majority of Fe atoms. However, the alignment of M_a of such atoms should strongly depend on the external magnetic field.

Comparing atomic structures of magnetic $LaFe_{13-x}Si_x$ (Fig. 1d) and NM LaFeSi (Fig. 1(a) insert), one can expect that $LaFe_{13-x}Si_x$ can precipitate in the LaFeSi matrix, coherently or not. The Curie temperature scales with the energy difference ΔE between PM and FM states (dashed line in Fig. 1(b)), which depends on the lattice constant, altered by strain or stress. Due to coherent strain, coherent precipitates undergo a FOMPT at T_C, which differs from incoherent precipitates. The NM LaFeSi matrix is inert to an external magnetic field, but the matrix can alter the magnetic response of coherent $LaFe_{13-x}Si_x$ precipitates. First, anisotropic thermal expansion of the matrix that adopts a tetragonal crystal structure should create variable stress fields around the precipitates. Second, large (up to 1.6 %) phase volume changes that occur in $LaFe_{13-x}Si_x$ at T_C will further modulate the stress fields locally. Coupled with the itinerant nature of the magnetism of $LaFe_{13-x}Si_x$, where both the magnetic moments and exchange interactions are sensitive to strain, both of these effects are expected to play a role in defining the magnetic responses of magnetically active $LaFe_{13-x}Si_x$ grains. Notably, as short-range order arising from two phases lowers energy, the actual energy per atom of the PM state will be lower than given by the DLM energy per atom. Consequently, the computed ΔE in Fig. 1(b) is an overestimate, albeit the slope vs. a is qualitatively correct. As M_a becomes smaller when the volume per atom is reduced and ΔE monotonically increases with M_a, starting from $\Delta E = 0$ at $M_a = 0$, the monotonic increase of $\Delta E(a)$ in Fig. 1(b) is expected.

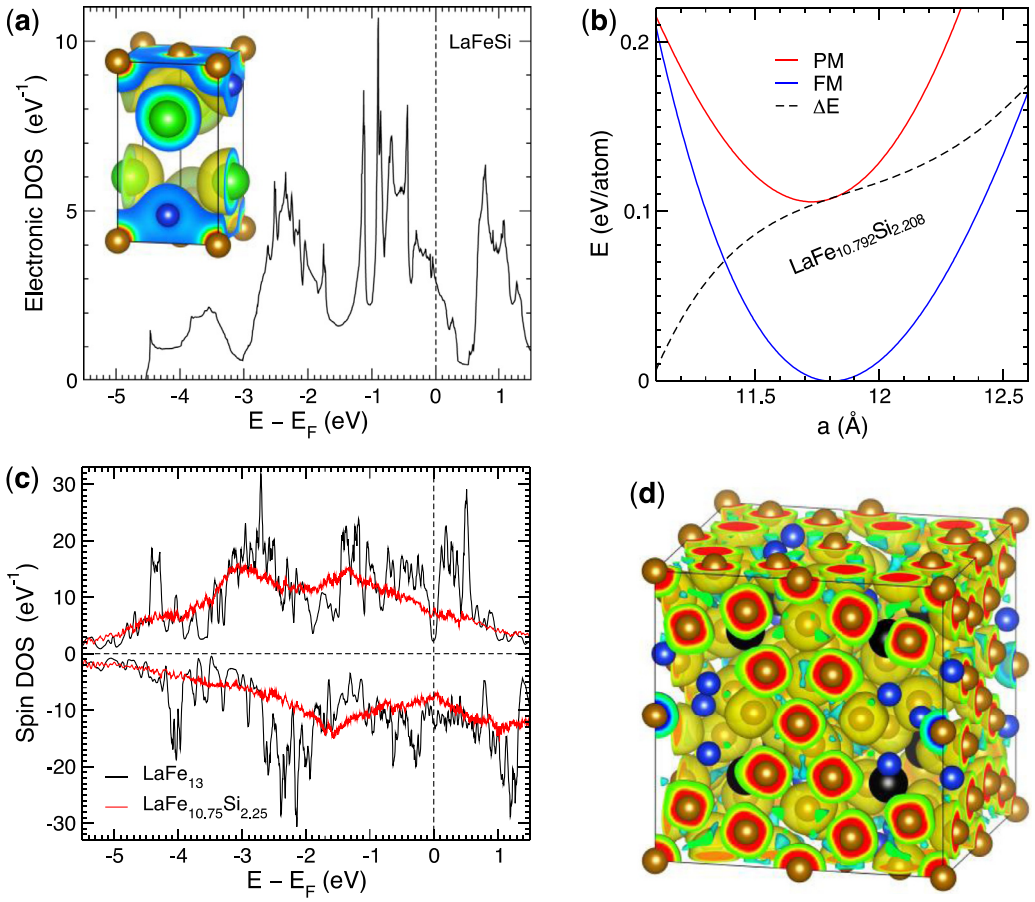

Fig. 1. (a) Calculated electronic DOS (states-eV^{-1} per formula unit) in non-magnetic LaFeSi. The inset shows 0.033 e/Å^3 charge-density isosurface in LaFeSi from VASP [La is green, Fe is brown, Si is blue]. (b) KKR-CPA energy of paramagnetic (PM DLM) and ferromagnetic (FM) states and ΔE = E(DLM) – E(FM) versus lattice constant in LaFe$_{13-x}$Si$_x$ at $x = 0$ and 2.208 with homogeneous disorder on (Fe,Si) sublattice. (c) Spin DOS (states-eV^{-1} per formula unit) in FM LaFe$_{13-x}$Si$_x$ at $x = 0$ and 2.25, computed in supercells using VASP. (d) 0.004 e/A^3 spin-density isosurfaces in FM LaFe$_{10.75}$Si$_{2.25}$ lowest-energy structure [La is black, Fe is brown, Si is blue]. Positive (up) spin density is red-yellow-green with yellow isosurface, negative (down) is shades of blue (high is dark, low is light) with light-blue isosurface.

From the distribution of Fe moments and the dependence of each atomic moment on its chemical environment (the fluctuating number of Si or Fe atoms among neighbors), we expect dependence of properties on the short-range order formed during heat treatment that depends on the thermal history of a sample. In particular, caloric response and T_C may differ in quenched and annealed samples. A similar effect was observed in other materials exhibiting a giant magnetocaloric effect [54].

5. Experimental results and discussion

Powder X-ray diffraction shows that $LaFe_2Si$ contains two phases (Fig. 2), where the minority (~20 wt.%) phase is $LaFe_{13-x}Si_x$ adopting the cubic $NaZn_{13}$-type structure and the majority (~80 wt.%) phase is $LaFeSi_{0.95}$ crystallizing in the PbClF-type structure with space group P4/nmm. The composition of the 1:13 phase was fixed with $x = 1.2$ (see below) and was not refined further, while the Rietveld refinement clearly indicates the presence of defects in the silicon sublattice of the majority phase (SI, Tables S2, and S3). According to XRD, the material contains no other phases, such as α-($Fe_{1-\delta}Si_\delta$), which is the primary solidification phase in alloys prepared at the $LaFe_{13-x}Si_x$ stoichiometry regardless of x [55,56], and is often present in nearly stoichiometric 1:13 alloys even after long term annealing. The SEM and EDX results, (Fig. S2, and Table S4, SI) are consistent with the XRD data, confirming the formation of a two-phase alloy, as well as the compositions of the two phases within the accuracy of the technique. Considering the average ratios of concentrations of Fe and Si in both phases determined from EDX, the LaFeSi matrix has stoichiometry close to $LaFeSi_{0.9}$, and stoichiometry of the $LaFe_{13-x}Si_x$ phase corresponds to $x = 1.21$. The latter nearly matches the commonly reported lowest concentrations of Si required to stabilize the $LaFe_{13-x}Si_x$ phase by annealing at and above 1300 K, while falling outside the homogeneity range of $LaFe_{13-x}Si_x$ at 873 K, which terminates at the lowest $x = 1.73$ [32].

The main $LaFeSi_{0.95}$ phase is a weak Pauli paramagnet with no reported magnetic or structural transitions down to 4.2 K [49]. Further, our DFT calculations return zero atomic magnetic moments for stoichiometric LaFeSi, which is consistent with the stable nonmagnetic phase of LaFeSi reported in ref. [57]. The absence of structural polymorphism in the matrix is confirmed by XRD data collected at 300 and 15 K (Fig. 2b). Therefore, $LaFeSi_{0.95}$ is expected to be a magnetically inert matrix contributing negligibly to the magnetization of the $LaFe_2Si$ composite; interactions between the two phases are expected to be nearly exclusively elastic. The minority $LaFe_{13-x}Si_x$ phase is distributed uniformly in the matrix, making the sample's microstructure uniquely adapted to exhibit functionalities that may not be available in a single-phase material, as discussed in detail below.

Heat capacity, $C_p(T)$, measurements of $LaFe_2Si$ in various magnetic fields are shown in Fig. 3. Unexpectedly, $C_p(T)$ displays two distinct anomalies: one at $T_1 = 154$ K, and another at $T_2 = 192$ K. Both anomalies clearly reflect the first-order nature of the underlying phase transformations. The anomaly at T_2 nominally cor-

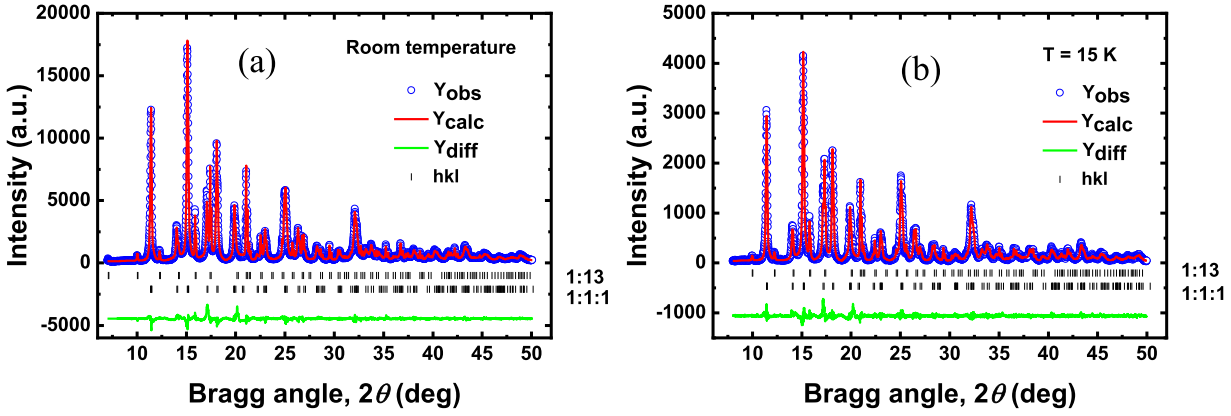

Fig. 2. Rietveld-refined X-ray powder diffraction patterns of $LaFe_2Si$ recorded at room temperature (a) and at T = 15 K (b). The upper sets of vertical bars represent locations of Bragg peaks of the minority cubic $NaZn_{13}$-type phase, and the bottom sets of vertical bars represent the same for the majority, PbClF-type phase.

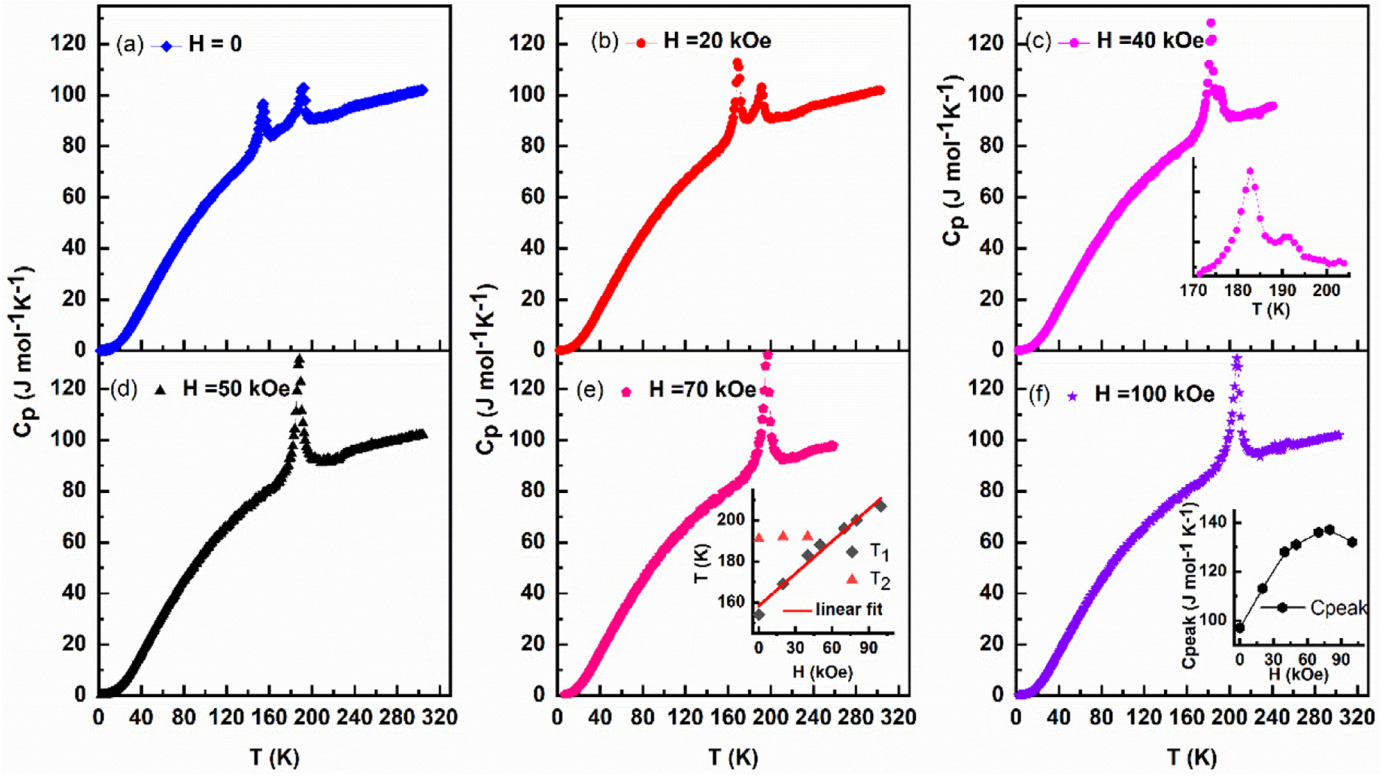

Fig. 3. Heat capacity, *Cp*, of $LaFe_2Si$ measured as a function of temperature in magnetic fields up to 100 kOe. Inset in (c) shows the details in the vicinity of the phase transition anomalies in H = 40 kOe. Inset in (e) shows temperatures of heat capacity peaks as functions of a magnetic field. Inset in (f) shows the peak values of the temperature-dependent heat capacity anomaly as a function of a magnetic field.

responds to ambient pressure T_C of $LaFe_{13-x}Si_x$ with $x = 1.45$ [27], but the lowest reported $T_C = 175$ K for $x = 1.17$ [27] is much higher than the observed T_1. Assuming that the linear dependence of ambient pressure T_C on x [27] holds for $x \leq 1.17$, $T_1 = 154$ K would indicate $x = 0.8$, which is impossible, considering both the XRD data of Fig. 2 and consistency of EDS results listed in Table S4. With the increasing magnetic field, the temperature of the $C_p(T)$ peak at T_1 increases rapidly and linearly, but the field has minimal, if any, effect on the anomaly at T_2, which remains distinguishable up to $H = 40$ kOe, remaining at the same $T_2 = 192$ K (Fig. 3e, inset). The two $C_p(T)$ anomalies merge at $H = 50$ kOe, and they remain together in higher magnetic fields. The field-dependent behavior of the anomaly at T_1, as well as of the single anomaly after the two merge at $H \geq 50$ kOe, is consistent with the effect of the magnetic field on IEM transitions in nearly phase-pure, chemically homogeneous $LaFe_{13-x}Si_x$. Hence, the splitting of the standard single IEM FOMPT and the unusual magnetic field-dependent behavior of the anomaly at T_2 in the active $LaFe_{13-x}Si_x$ component of the composite must be related to the mechanical coupling with the magnetically inert matrix.

As commonly observed in intermetallic compounds that exhibit robust first-order magnetoelastic transitions, the individual anomalies at T_1 and T_2, and the single anomaly after the two merge, remain quite sharp regardless of the magnetic field. As T_1 (and T_2 after the two peaks merge) increases with the magnetic field, the magnitude of the heat capacity peak increases, as expected assuming that the total entropy change during the corresponding phase transformation remains constant. Only at 100 kOe the single heat capacity anomaly begins to noticeably broaden, as follows from the reduction of the peak maximum (see inset in Fig. 3f). The value of

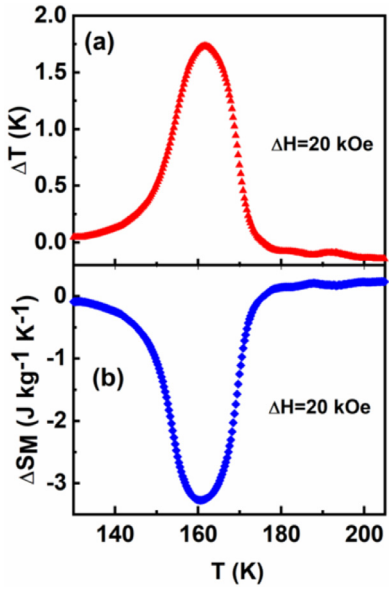

Fig. 4. The adiabatic temperature change (a) and the magnetic field induced entropy change (b) as functions of temperature computed from heat capacity data for $\Delta H = 20$ kOe.

$C_p(T = 300\ \text{K}) = 101$ J mol^{-1} K^{-1} in zero magnetic field (Fig. 3a) is in agreement with the classical Dulong and Petit limit of the lattice heat capacity at constant volume $C_V = 3nR = 99.77$ J mol^{-1} K^{-1}, where n = 4 is the number of atoms per $LaFe_2Si$ formula unit, and R is the universal gas constant [28].

The maximum adiabatic temperature change (ΔT) and maximum magnetic field induced entropy change (ΔS_M) computed from the heat capacity data of Fig. 3 and illustrated in Fig. 4 for $\Delta H = 20$ kOe, are 1.7 K and -3.3 J kg^{-1} K^{-1}, respectively. Considering that only *ca* 20 wt. % of the 1:13 constituent is present in the title material, the actual maximum value of the magnetic entropy change in the active $LaFe_{13-x}Si_x$ phase is at least -16.5 J kg^{-1} K^{-1}, which is comparable to the reported maximum ΔS_M of pure phases, for example, -21.2, -20.8, and -14.2 J kg^{-1} K^{-1} for x = 1.17 and 1.4, and 1.6, respectively, for the same magnetic field change of 20 kOe [27].

The full-widths at half maxima (FWHMs) of ΔT vs. T and ΔS_M vs. T curves are ~17 K at $\Delta H = 20$ kOe (~38 K for ΔS_M vs. T at $\Delta H = 50$ kOe, see Fig. 5b, below), which represents an extraordinary enhancement when compared to approximately 5 K (21 K) FWHMs observed in nearly phase pure $LaFe_{13-x}Si_x$ [27] for the same $\Delta H = 20(50)$ kOe. Thus, our results suggest that both the nature of the matrix and the distribution of the magnetocalorically active $LaFe_{13-x}Si_x$ phase in the matrix represent heretofore unrecognized, highly effective tools for controlling the progression of the magnetic field-induced first-order phase transition, related magnetocaloric effect and, likely, other physical properties of this and similar composites.

The isothermal magnetization, $M(H)$, measured in the vicinity of both T_1 and T_2 and illustrated in Fig. 5a is in agreement with the heat capacity data of Fig. 3. Field-induced metamagnetic-like transitions are observed above T_1 with the critical fields rapidly rising as temperature increases from 153 to 181 K. Magnetic fields below 50 kOe are too low to complete the transition at 185 and 189 K, and at $T = 193$ K (just above the zero field T_2) $M(H)$ becomes practically linear. Fig. 5b depicts the magnetic field induced entropy changes computed from the magnetization data for magnetic field changes up to 50 kOe. Noting that $\Delta S_M(T)$ for $\Delta H = 20$ kOe is in good agreement with the same calculated from the heat capacity data o Fig. 4, the peak ΔS_M values vary from -2.2 J kg^{-1} K^{-1} to -4.2 J kg^{-1} K^{-1} at $\Delta H = 10$ and 50 kOe, respectively, and FWHM of ΔS_M vs T reaches ~38 K at $\Delta H = 50$ kOe.

The low-field ($H = 1$ kOe) magnetization, $M(T)$, (Fig. 6a) shows a single step-like anomaly at $T_C = 144$ K on cooling (taken as the minimum of dM/dT function), closely matching zero-field T_1, which moves to 186 K when the magnetic field increases to 50 kOe; the heating and cooling $M(T)$ data show anhysteretic phase transition in $H = 50$ kOe (Fig. 6a). The anomaly in $C_p(T)$ observed at T_2 is not reflected in low-field $M(T)$. The inverse dc magnetic susceptibility shows two distinct temperature-dependent regimes (Fig. 6b and Fig. S3, SI): above approximately 250 K it follows the Curie-Weiss law, but at lower temperatures, an obvious downturn signals the onset of a Griffiths phase-like behavior below a characteristic temperature, T_G. The emergence of the Griffiths phase is usually associated with short-range FM clustering due to chemical inhomogeneities, but in the case of $LaFe_2Si$ it may also be related to the effects of strain existing at the likely incoherent interfaces between the nonmagnetic LaFeSi matrix and magnetic $LaFe_{13-x}Si_x$ inclusions.

To further understand the unusual twin anomalies observed in the heat capacity, the absence of the anomaly corresponding to T_2 in $M(T)$ data, and to analyze the associated crystallographic changes, we carried out a temperature-dependent, powder X-ray diffraction study of $LaFe_2Si$ between 15 and 300 K in 0 to 35 kOe applied magnetic fields. Upon cooling in zero magnetic field (Fig. 7a), the Bragg peaks of $LaFe_{13-x}Si_x$ rapidly but gradually begin to shift to lower Bragg angles, starting around 190 K (close to the transition at T_2), consistent with a strong lattice expansion. These changes are followed by the discontinuous shifts of the same Bragg peaks between 170 and 160 K, confirming that the IEM transition in $LaFe_{13-x}Si_x$ is magnetoelastic and first order. Note that, when recorded in a 35 kOe magnetic field (Fig. 7b), the discontinuous changes of the positions of Bragg peaks of $LaFe_{13-x}Si_x$ occur around 190 K, approximately coinciding with the temperature where the continuous lattice expansion on cooling in zero magnetic field is the fastest (also see next paragraph), in agreement with the observed field-induced merging of the two heat capacity peaks. The Bragg peaks of the $LaFeSi_{0.95}$ matrix, on the other hand, shift gradually and weakly in both 0 and 35 kOe magnetic fields, in accordance with the conventional lattice contraction on cooling.

The temperature dependencies of the lattice parameters in 0 and 35 kOe magnetic fields are illustrated in Figs. 7c, d. As mentioned above, the application of a 35 kOe field increases the temperature of the discontinuous lattice parameter change in $LaFe_{13-x}Si_x$ from ~165 K to ~190 K. At the same time, lattice parameters of $LaFeSi_{0.95}$ decrease monotonically with temperature and are practically unaffected by the magnetic field. Thus, we conclude that the observed anomalies in the physical behaviors of the $LaFe_2Si$ alloy correlate with the lattice changes of the $LaFe_{13-x}Si_x$ phase, while the elastic behavior of the $LaFeSi_{0.95}$ matrix is conventional. A closer examination of Fig. 7c shows that the zero-field dependence of a for $LaFe_{13-x}Si_x$ has two anomalies – the first-order discontinuity at $T_C \cong T_1$, and a rapid change that occurs around 190 K, corresponding to T_2. Comparison of the structural information for room temperature and 15 K (Tables S2, and S3, SI) provides no indication of a structural change, other than the well-documented magnetovolume effect in the $LaFe_{13-x}Si_x$ phase. Considering all of the data discussed so far, the formation of the $LaFeSi_{0.95}/LaFe_{13-x}Si_x$ composite splits the phase transformation in $LaFe_{13-x}Si_x$ into two related events: a strongly first-order, discontinuous transition around T_1 reflected in heat capacity, crystallographic, and magnetic data, plus a weakly first-order transition around T_2 detectable by heat capacity and crystallography. Application of the magnetic field of ~50 kOe and higher leads to a single discontinuous IEM.

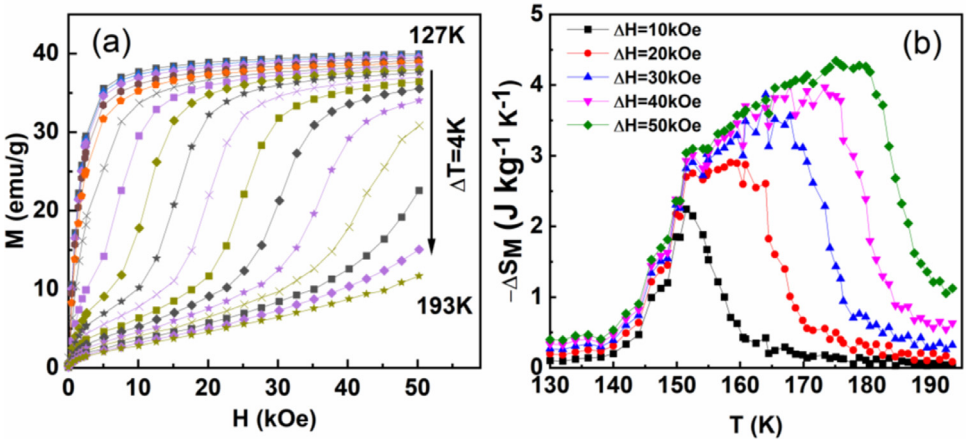

Fig. 5. (a) Isothermal magnetization measured between 127 K and 193 K in applied magnetic fields up to 50 kOe. (b) Magnetic field induced entropy changes as functions of temperature for magnetic field changes ranging between 10 and 50 kOe calculated from the magnetization data of (a).

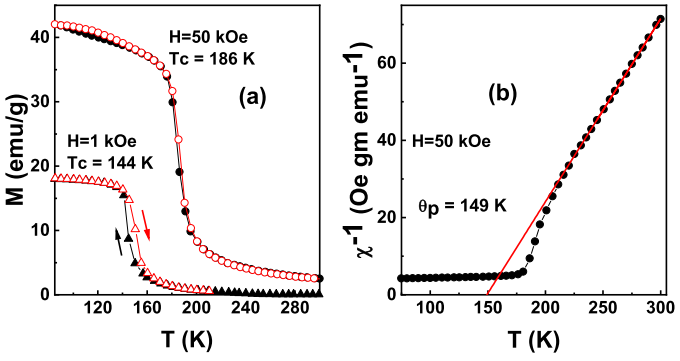

Fig. 6. (a) Magnetization of $LaFe_2Si$ measured on heating (open symbols) and cooling (closed symbols) in 1 and 50 kOe magnetic fields. (b) Inverse DC magnetic susceptibility of $LaFe_2Si$ and the Curie-Weiss fit.

The room-temperature Mössbauer spectrum of $LaFe_2Si$ is shown in Fig. 8a and it can be fitted with a doublet and a singlet with areas of 56(1)% and 44(1)%, respectively. This corresponds to approximately 25 vol.% of the $LaFe_{11.8}Si_{1.2}$ and 75 vol.% of the $LaFeSi_{0.95}$ phases in the $LaFe_2Si$ alloy (28 and 72 wt.%, respectively, accounting for the differences in the X-ray densities of the two phases, which are 7.3 and 6.1 g/cm^3), in good agreement with SEM (Fig. S2) and powder XRD (Table S2) results. Cooling $LaFe_2Si$ yields a magnetic contribution that is initially quite broad and gradually sharpens upon further cooling, reaching its final form around 175 K (Fig. 8b). However, even at 10 K the magnetic component is clearly broadened with the Gaussian distribution of hyperfine fields peaked at 33.7(3) T typical for metallic iron, with widths of 2.1(2) T and 4.3(2) T to the high and low sides, respectively. Plotting the temperature dependence of the magnetic fraction in the ^{57}Fe Mössbauer spectra (Fig. 8c) shows that the transition at 195 K is first-order. However, cycling through the transition shows no evidence for significant hysteresis (<5 K). The temperature dependence of the average hyperfine field (<B_{hf}>) in Fig. 8d shows two distinct regimes. Between the onset at 195 K and 175 K, there is a rapid growth in <B_{hf}>, and the distribution of fields also sharpens up. Below 175 K, <B_{hf}> follows a more conventional form and, as Fig. 8d (dashed-line) shows it can be fitted using an S = 1/2 Brillouin function yielding an extrapolated ordering temperature of 279(1) K - the ordering temperature of the low-T form that would be observed if the first-order magnetovolume transition did not intervene. Estimated from <B_{hf}>, the mean magnetic moment of Fe reaches 2.1 μ_B/atom, which is in an excellent agreement with the individual atomic moments predicted from DFT (Table S1) assuming collinear ferromagnetism and $x = 1.2$ stoichiometry.

The appearance of the magnetic fraction in the ^{57}Fe Mössbauer spectra is commensurate with the first-order nature of the phase transition at T_2 seen in heat capacity, yet the magnetic transition itself is not reflected in $M(T)$ data. Further, our ac magnetic susceptibility data (Fig. S3, SI) demonstrate that energy losses related to domain wall motion and domain magnetization rotation, reflected by non-zero out of phase (imaginary) component, emerge at T_1 but they are absent between T_1 and T_2. Considering conventional thermal expansion between 200 and 300 K (Fig. 7), $\Delta a/a$ of both phases are of the same orders of magnitude, ~8.7 and ~6.1 ppm K^{-1} for the $LaFe_{13-x}Si_x$ and $LaFeSi_{0.95}$, respectively. The thermal expansion of the latter is anisotropic, and its $\Delta c/c \cong 17$ ppm K^{-1} is much higher. Elastic coupling between the matrix and the 1:13 phase, therefore, brings anisotropic stress to bear on the progression of the normally single step IEM FOMPT in $LaFe_{13-x}Si_x$. Complex interplay between the effect of local strain fields on the development of IEM that goes beyond a similar analysis of the same in a millimeter-size, unconstrained $LaFe_{13-x}Si_x$ grains [58] requires further studies, but it is clear that the rapid lattice expansion on cooling around T_2 observed in powder XRD data of Fig. 7, gets arrested before T_1. Hence the rapid development of the hyperfine field (and iron magnetic moments) between T_2 and T_1 remains hidden in bulk dc magnetization and ac magnetic susceptibility measurements due to demagnetizing fields that are functions of both magnetization and stress [59].

The electrical resistivity as a function of temperature and magnetic field between 1.8 and 300 K is shown in Fig. 9. During the resistivity measurements, the sample was cycled through IEM FOPT over 20 times by heating and cooling between 2 to 325 K in the fields ranging from 0 to 100 kOe. For each magnetic field, the resistivity curves above and below the phase transition overlap, suggesting the sample is mechanically stable, with no cracks developing, and unaffected by aging due to thermal and magnetic cycling. As is well known, $LaFe_{13-x}Si_x$ and, especially, its hydrides are mechanically unstable and their functional properties degrade even after a few cycles at a low field [3]. Therefore, $LaFe_{13-x}Si_x$ based materials require a binder for applications [30]. The residual resistivity is 6 μΩ-cm, which is low for polycrystalline samples, and this value does not change with thermal cycling or magnetic field. The resistivity increases with temperature, indicating metallic behavior. The anomalous step in resistivity is observed at $T_C = 154$ K in zero magnetic field, confirming the first-order nature of the

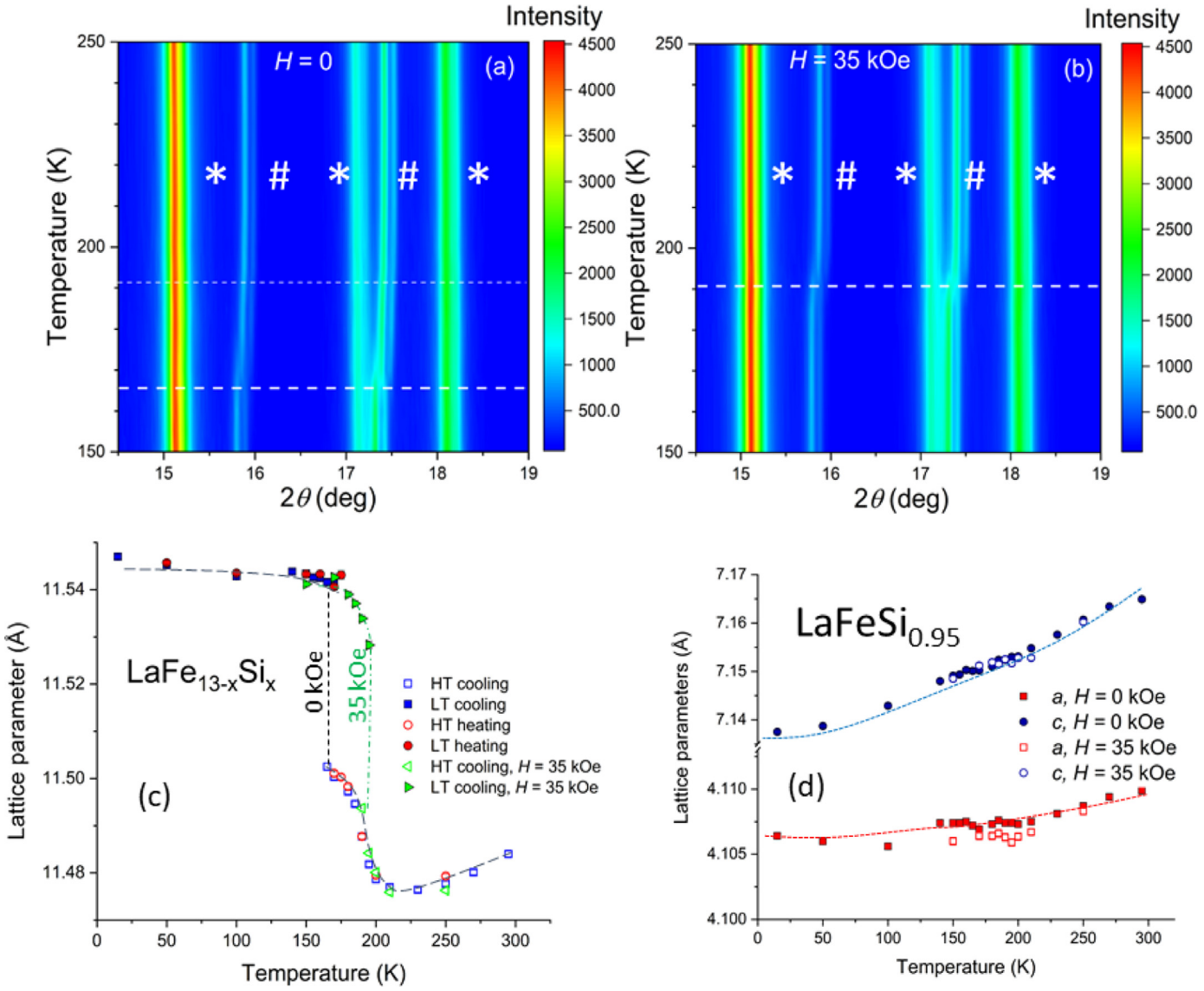

Fig. 7. The intensity contour maps of the x-ray diffraction patterns of $LaFe_2Si$, shown in the region $14.5° \leq 2\theta \leq 19°$ for clarity, measured upon cooling in H=0 (a) and 35 kOe (b). The (*) and (#) symbols in (a) and (b) represent the $LaFeSi_{0.95}$ and $LaFe_{13-x}Si_x$ phases, respectively. The unit-cell dimensions as functions of temperature at H = 0 and 35 kOe of $LaFe_{13-x}Si_x$ (c) and $LaFeSi_{0.95}$ (d) phases determined from Rietveld refinements.

transition, shifting up to ~212 K in a 100 kOe field (Fig. 9a, inset). The temperatures of the steps in the electrical resistivity are consistent with the $C_p(T)$ peaks at T_1 and the single $C_p(T)$ peak observed in fields higher than 40 kOe. Like bulk magnetization, no significant change in electrical resistivity occurs at T_2, which could be due to the weakly first-order nature of the phase transition, or geometry and lack of the connectivity between precipitates of the $LaFe_{13-x}Si_x$ phase.

Magnetoresistance, defined as MR = $[\rho(H,T)$ - $[\rho(0,T)]/[\rho(0,T)] \times 100\%$ reaches +8% over a broad temperature interval with FWHM of 16 K for ΔH = 20 kOe (Fig. 9b). The maximum values of MR do not change significantly in higher magnetic fields, however, FWHM increases to ~32 K in H = 50 kOe, which is consistent with the dT_1/dH of ~ 0.8 K/kOe. The broad temperature ranges over which substantial MR is observed are consistent with equally broad temperature ranges where the giant magnetocaloric effects are observed in the same magnetic field changes. The plateaus in MR, ΔT and ΔS_M occurring in wide temperature ranges, though rarely observed, are very important for applications.

6. Conclusions

We report the anomalous physical properties of the $LaFe_2Si$ alloy, a naturally formed composite containing two phases: magnetically inactive $LaFeSi_{0.95}$ matrix phase and an active $LaFe_{13-x}Si_x$ inclusion phase. In addition to nearly *anhysteretic, yet sharply first-order and strongly magnetic field-dependent* phase transition at T_1 that coincides with the Curie temperature, T_C, an unexpected magnetic-field-independent, a first-order transition occurs at a higher T_2. This composite system exhibits highly *non-linear giant magnetocaloric effect and large positive magnetoresistance* near T_C that are effective over the range of temperatures 2-3 times broader than the same in nearly phase pure $LaFe_{13-x}Si_x$. Further, the Curie temperature of the active component of the composite is highly sensitive to a magnetic field, where $\partial T_C/\partial H$ = 0.85 K kOe^{-1}, which is a critical parameter establishing a fundamen-

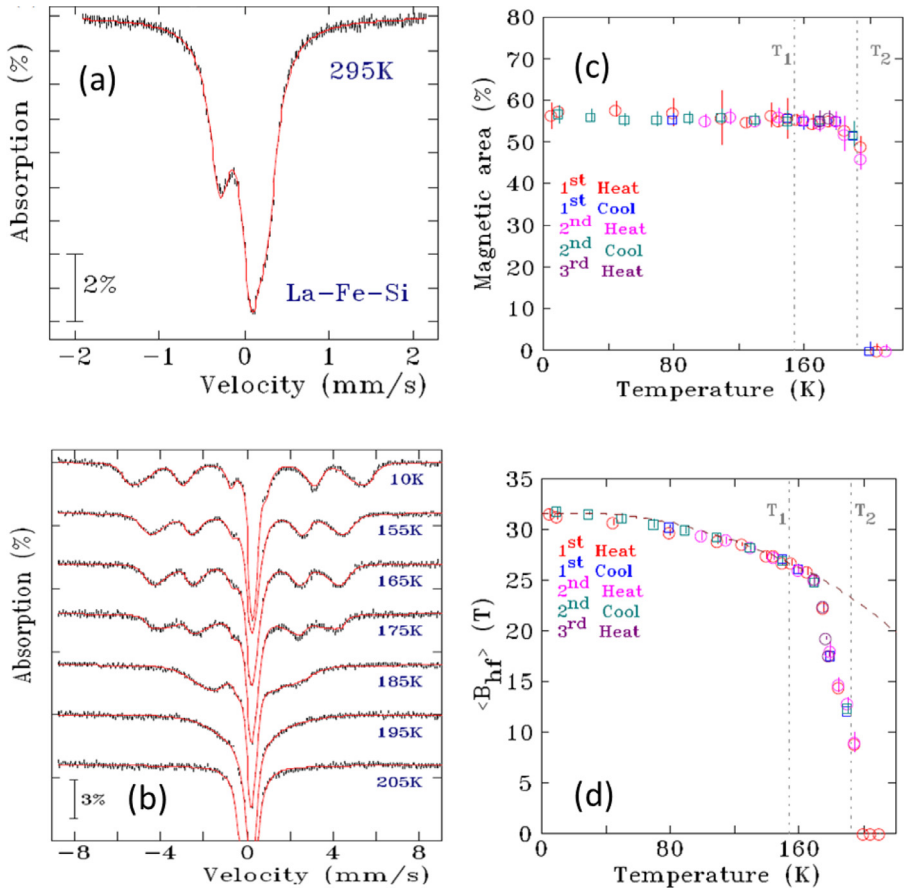

Fig. 8. (a) Room temperature and (b) low temperature ^{57}Fe Mössbauer spectra of $LaFe_2Si$. (c) Temperature dependence of the magnetic fraction in the ^{57}Fe Mössbauer spectra of $LaFe_2Si$ showing the discontinuous onset on cooling through 195 K. (d) Temperature dependence of the average hyperfine field (<Bhf>) in the ^{57}Fe Mössbauer spectra of $LaFe_2Si$ showing the discontinuous onset on cooling through 195 K. Below 175 K the behavior can be fitted using an S = 1/2 Brillouin function (dashed line) yielding an extrapolated ordering temperature of 279(1) K.

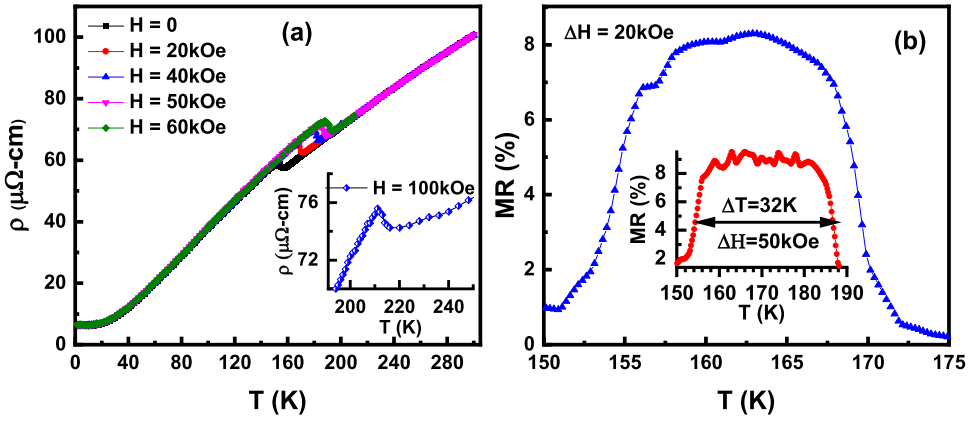

Fig. 9. The resistivity, ρ, as a function of temperature measured in magnetic fields up to 60 kOe (a). Inset in (a) shows ρ(T) near the phase transition for H = 100 kOe. The magnetoresistance, MR, as a function of temperature at ΔH = 20 kOe (b). Inset in (b) shows MR vs. temperature for ΔH = 50 kOe.

tal limit on the maximum possible adiabatic temperature change. Magnetic fields as high as 100 kOe do not weaken the first-order phase transition at T_C, whereas, in other IEM systems, like FeRh, it is strongly suppressed by an increasing field. All anomalies in the physical properties correlate with the lattice changes of the $LaFe_{13-x}Si_x$ phase, while the crystallographic behavior of the LaFeSi phase is conventional in the examined range of temperatures and magnetic fields. Obviously, the LaFeSi matrix strongly modifies the physical behavior of the $LaFe_{13-x}Si_x$, while itself remaining indifferent to the external stimuli beyond conventional thermal expansion. Both experiment and theory show that the LaFeSi matrix is NM, but it alters the magnetic response of the $LaFe_{13-x}Si_x$ precipitates. This discovery of a thermodynamically stable composite system (ferromagnetic phase embedded in the non-magnetic phase)

opens new avenues for the design of multifunctional intermetallic magnetic materials.

Declaration of Competing Interest

The authors declare that they have no known competing financial interests or personal relationships that could have appeared to influence the work reported in this paper.

Acknowledgments

This work was performed at the Ames Laboratory and was funded by the U.S. Department of Energy (DOE), Office of Science, Office of Basic Energy Sciences, Materials Sciences and Engineering Division. The Ames Laboratory is operated for the U. S. DOE by Iowa State University under contract No. DE-AC02-07CH11358. DHR acknowledges Fonds Québécois de la Recherche sur la Nature et les Technologies for financial support for Mössbauer spectroscopy. A part of the magnetic measurement was performed at Buffalo State College. A.K.P. acknowledges financial support from the SUNY, Buffalo State Incentive Award, and start-up fund to finalize the work.

Supplementary materials

Supplementary material associated with this article can be found, in the online version, at doi:10.1016/j.actamat.2021.117083.

References

[1] V.K. Pecharsky, K.A. Gschneidner Jr., Giant magnetocaloric effect in $Gd_5(Si_2Ge_2)$, Phys. Rev. Lett. 78 (1997) 4494.
[2] S. Fujieda, A. Fujita, K. Fukamichi, Large magnetocaloric effect in $La(Fe_xSi_{1-x})_{13}$ itinerant-electron metamagnetic compounds, Appl. Phys. Lett 81 (2002) 1276.
[3] J. Lyubina, R. Schäfer, N. Martin, L. Schultz, O. Gutfleisch, Novel design of $La(Fe,Si)_{13}$ alloys towards high magnetic refrigeration performance, Adv. Mater. 22 (2010) 3735.
[4] J. Liu, Chun He, M.X. Zhang, A.R. Yan, A systematic study of the microstructure, phase formation and magnetocaloric properties in off-stoichiometric La-Fe-Si alloys, Acta Mater 118 (2016) 44.
[5] E. Lovell, A.M. Pereira, A. David Caplin, J. Lyubina, L.F. Cohen, Dynamics of the first-order metamagnetic transition in magnetocaloric $La(Fe,Si)_{13}$: Reducing hysteresis, Adv. Energy Mater. 5 (2015) 1401639 2015.
[6] M. Bratko, K. Morrison, A. de Campos, S. Gama, L.F. Cohen, K.G. Sandeman, History dependence of directly observed magnetocaloric effects in (Mn,Fe)As, Appl. Phys. Lett. 100 (2012) 252409.
[7] G.A. Govor, V.I. Mitsiuk, S.A. Nikitin, N.Yu. Pankratov, A.I. Smarzhevskaya, Magnetostructural phase transitions and magnetocaloric effect in Mn(As,P) compounds and their composites, J. Alloys Compd. 801 (2019) 428.
[8] S. Stadler, M. Khan, J. Mitchell, N. Ali, A.M. Gomes, I. Dubenko, A.Y. Takeuchi, A.P. Guimarães, Magnetocaloric properties of $Ni_2Mn_{1-x}Cu_xGa$, Appl. Phys. Lett. 88 (2006) 192511.
[9] S. Jacobs, A.Boeder J.Auringer, L.Komorowski J.Chell, J. Leonard, S. Russek, C. Zimm, The performance of a large-scale rotary magnetic refrigerator, Intern. J. Refriger. 37 (2014) 84.
[10] V.K. Pecharsky, J. Cui, D.D. Johnson, Magneto)caloric refrigeration: Is there light at the end of the tunnel? Phil. Trans. R. Soc. A 374 (2016) 20150305.
[11] C. Zimm, A. Boeder, B. Mueller, K. Rule, S.L. Russek, The evolution of magnetocaloric heat-pump devices, MRS Bull. 43 (274) (2018).
[12] N.T Trung, V. Biharie, L. Zhang, L. Caron, K.H.J. Buschow, E Brück, From single- to double-first-order magnetic phase transition in magnetocaloric compounds, Appl. Phys. Lett. 96 (2010) 162507.
[13] L. Mañosa, D. González-Alonso, A. Planes, M. Barrio, Josep-Lluís Tamarit, I.S. Titov, M. Acet, A. Bhattacharyya, S. Majumda, Inverse barocaloric effect in the giant magnetocaloric La– Fe – Si– Co compound, Nat. Comm. 2 (2011) 595.
[14] J. Liu, Y. Gong, Y. You, X. You, B. Huang, X. Miao, G. Xu, F. Xu, E. Brück, Giant reversible magnetocaloric effect in MnNiGe-based materials: Minimizing thermal hysteresis via crystallographic compatibility modulation, Acta Mat. 174 (2019) 450e458.
[15] P. Lloveras, T. Samanta, M. Barrio, I. Dubenko, N. Ali, J. Tamarit, S. Stadler, Giant reversible barocaloric response of $(MnNiSi)_{1-x}(FeCoGe)_x$ (x = 0.39, 0.40, 0.41), APL. Mater. 7 (2019) 061106.
[16] T. Samanta, P. Lloveras, A. Us Saleheen, D.L. Lepkowski, E. Kramer, I. Dubenko, P.W. Adams, D.P. Young, M. Barrio, J. Ll. Tamarit, N. Ali, S. Stadler, Barocaloric and magnetocaloric effects in $(MnNiSi)_{1-x}(FeCoGe)_x$, Appl. Phys. Lett. 112 (2018) 021907.
[17] J. Liu, Y. Gong, G. Xu, Guo Peng, I.A. Shah, N. ul Hassan, F. Xu, Realization of magnetostructural coupling by modifying structural transitions in MnNiSi–CoNiGe system with a wide Curie-temperature window, Sci. Rep. 6 (2016) 23386.
[18] A. Biswas, Y. Mudryk, A.K Pathak, L. Zhou, V.K Pecharsky, Managing hysteresis of $Gd_5Si_2Ge_2$ by magnetic field cycling, J. App. Phys. 126 (2019) 243902.
[19] S. Fujieda, A. Fujita, K. Fukamichi, Y. Yamazaki, Y. Iijima, Giant isotropic magnetostriction of itinerant-electron metamagnetic $La(Fe_{0.88}Si_{0.12})_{13}H_y$ compounds, Appl. Phys. Lett. 79 (2001) 653.
[20] J. Hao, F. Hu, Jian-Tao Wang, Fei-Ran Shen, Z. Yu, H. Zhou, H. Wu, Q. Huang, K. Qiao, J. Wang, J. He, L. He, Ji-Rong Sun, B. Shen, Large enhancement of magnetocaloric and barocaloric effects by hydrostatic pressure in $La(Fe_{0.92}Co_{0.08})_{11.9}Si_{1.1}$ with a $NaZn_{13}$-type structure, Chem. Mater. 32 (2020) 1807.
[21] M. Phejar, V. Paul-Boncour, L. Bessais, Investigation on structural and magnetocaloric properties of, $LaFe_{13-x}Six(H,C)y$ compounds, J. Solid State Chem. 233 (2016) 95.
[22] A. Terwey, M.E. Gruner, W. Keune, J. Landers, S. Salamon, B. Eggert, K. Ollefs, V. Brabänder, I. Radulov, K. Skokov, T. Faske, M.Y. Hu, J. Zhao, E.E. Alp, C. Giacobbe, O. Gutfleisch, H. Wende, Influence of hydrogenation on the vibrational density of states of magnetocaloric $LaFe_{11.4}Si_{1.6}H_{1.6}$, Phys. Rev. B 101 (2020) 064415.
[23] F. Wang, G. Wang, F. Hu, A. Kurbakov, B. Shen, Z. Cheng, Strong interplay between structure and magnetism in the giant magnetocaloric intermetallic compound $LaFe_{11.4}Si_{1.6}$: a neutron diffraction study, J. Phys.: Condes. Matter 15 (2003) 5269.
[24] L.B. Xu, Z Altounian, D.H. Ryan, Structure and magnetic transition of $LaFe_{13-x}Six$ compounds, J. Phys.: Condes. Matter 15 (2003) 7385.
[25] A. Fujita, K. Fukamichi, Control of large magnetocaloric effects in metamagnetic $La(Fe_xSi_{1x})_{13}$ compounds by hydrogenation, J. Alloys Compd. 404 (2005) 554.
[26] Y. Sun, Z. Arnold, J. Kamarad, Guang-Jun Wang, Bao-Gen Shen, Zhao-Hua Cheng, Pressure enhancement of the giant magnetocaloric effect in $LaFe_{11.6}Si_{1.4}$, Appl. Phys. Lett. 89 (2006) 172513.
[27] B.G. Shen, J.R. Sun, F.X. Hu, H.W. Zhang, Z.H. Cheng, Recent progress in exploring magnetocaloric materials, Adv. Mater. 21 (2009) 4545.
[28] C. Kittel, Introduction to Solid State Physics, 8th ed., Wiley, New York, 2005.
[29] A.K. Pathak, P. Basnyat, I. Dubenko, S. Stadler, N. Ali, Influence of the small substitution of Z = Ni, Cu, Cr, V for Fe on the magnetic, magnetocaloric, and magnetoelastic properties of $LaFe_{11.4}Si_{1.6}$, J. Magn. Magn. Mater. 322 (2010) 692.
[30] W.B. Fan, Y.H. Hou, X.J. Ge, Y.L. Huang, J.M. Luo, Z.C. Zhong, Microstructure and improved magnetocaloric properties: LaFeSi/LaAl magnets prepared by spark plasma sintering technique, J. Phys. D: Appl. Phys. 51 (2018) 115003.
[31] YiXu Wang, H. Zhang, EnKe Liu, XiChun Zhong, Kun Tao, MeiLing Wu, ChengFen Xing, YaNing Xiao, Jian Liu, Yi Long, Outstanding comprehensive performance of $La(Fe,Si)_{13}H_y$/In composite with durable service life for magnetic refrigeration, Adv. Electron. Mater. 4 (2018) 1700636.
[32] O.I. Bodak, E.I. Gladyshevskii, The lanthanum-iron-silicon system, Visn. Lviv Derzh. Univ. Ser. Khim. 14 (1972) 29.
[33] Mi-Kyung Han, G.J. Miller, An application of the "Coloring problem": Structure-composition-bonding relationships in the magnetocaloric materials $LaFe_{13-x}Si_x$, Inorg. Chem. 47 (2008) 515.
[34] K. Lowe, J. Liu, K. Skokov, J.D. Moore, H. Sepehri-Amin, K. Hono, M. Katter, O. Gutfleisch, The effect of the thermal decomposition reaction on the mechanical and magnetocaloric properties of $La(Fe,Si,Co)_{13}$, Acta Mater 60 (2012) 4268.
[35] A.P. Holm, V.K. Pecharsky, K.A. Gschneidner Jr., R. Rink, M. Jirmanus, X-ray powder diffractometer for *in situ* structural studies in magnetic fields from 0 to 35 kOe between 2.2 and 315 K, Rev. Sci. Instrum. 75 (2004) 1081.
[36] B. Hunter, Rietica – A visual Rietveld program, Int. Union Crystallogr. Commission Powder Diffraction Newslett. No 20 (1998) (Summer) [http://www.rietica.org].
[37] V.K. Pecharsky, J.O. Moorman, K.A. Gschneidner Jr., A 3–350 K fast automatic small sample calorimeter, Rev. Sci. Instrum. 68 (1997) 4196.
[38] G. Kresse, J. Hafner, Ab initio molecular dynamics for liquid metals, *Ab initio* molecular dynamics for liquid metals, Phys. Rev. B 47 (1993) 558(R).
[39] G. Kresse, J. Hafner, Ab initio molecular-dynamics simulation of the liquid-metal –amorphous-semiconductor transition in germanium, Phys. Rev. B 49 (1994) 14251.
[40] D.D. Johnson, A.V. Smirnov, William A. Shelton, S.N. Khan, MECCA: Multiple-scattering electronic-structure calculations for complex alloys. KKR-CPA program, Ver. 2.0, Iowa State University and Ames Laboratory, Ames, 2015.
[41] D.D. Johnson, D.M. Nicholson, F.J. Pinski, B.L. Gyorffy, G.M. Stocks, Density–functional theory for random alloys: Total energy within the coherent-potential approximation, Phys. Rev. Lett. 56 (1986) 2088.
[42] J.P. Perdew, K. Burke, M. Ernzerhof, Generalized gradient approximation made simple, Phys. Rev. Lett. 77 (1996) 3865.
[43] D.D. Johnson, Modified Broyden's method for accelerating convergence in self-consistent calculations, Phys. Rev. B 38 (1988) 12807.
[44] H.J. Monkhorst, J.D. Pack, Special points for Brillouin-zone integrations, Phys. Rev. B 13 (1976) 5188.
[45] K. Persson, Materials Project, Materials Data on LaFeSi by Materials Project. (2020) United States, doi:10.17188/1262485.
[46] D.D. Johnson, D.M. Nicholson, F.J. Pinski, B.L. Gyorffy, G.M. Stocks, Density–functional theory for random alloys: Total energy within the coherent-potential approximation, Phys. Rev. B 41 (1990) 9701.
[47] D.D. Johnson, F.J. Pinski, Inclusion of charge correlations in calculations of the energetics and electronic structure for random substitutional alloys, Phys. Rev. B 48 (1993) 11553.
[48] http://theory.cm.utexas.edu/henkelman/code/bader/

[49] R. Welter, G. Venturini, B. Malaman, Magnetic properties of RFeSi (R = La-Sm, Gd-Dy) from susceptibility measurements and neutron diffraction studies, J. Alloys Compd. 189 (1992) 49.
[50] N.A. Zarkevich, D.D. Johnson, Reliable thermodynamic estimators for screening caloric materials, J. Alloys Compd. 802 (2019) 712.
[51] A. Biswas, N.A. Zarkevich, A.K Pathak, O. Dolotko, I.Z Hlova, A.V. Smirnov, Y. Mudryk, D.D. Johnson, V.K Pecharsky, First-order magnetic phase transition in Pr_2In with negligible thermomagnetic hysteresis, Phy. Rev. B 101 (2020) 224402.
[52] P. Singh, A.V. Smirnov, A. Alam, D.D. Johnson, First-principles prediction of incipient order in arbitrary high-entropy alloys: exemplified in $Ti_{0.25}$CrFeNiAlx, Acta Mater 189 (2020) 248.
[53] Mi-Kyung Han, Ya-Qiao Wu, M. Kramer, B. Vatovez, F. Grandjean, G.J. Long, G.J. Miller, Superstructure in $RE_{2-x}Fe_4Si_{14-y}$ (RE = Y, Gd−Lu) characterized by diffraction, electron microscopy, and Mössbauer spectroscopy, Inorg. Chem. 45 (2006) 10503.
[54] S. Nikitin, G. Myalikgulyev, A. Tishin, M. Annaorazov, K. Asatryan, A. Tyurin, The magnetocaloric effect in $Fe_{49}Rh_{51}$ compound, Phys. Lett. 148 (1990) 363.
[55] Feng-xia Hu, Bao-gen Shen, Ji-rong Sun, Zhao-hua Cheng, Influence of negative lattice expansion and metamagnetic transition on magnetic entropy change in the compound $LaFe_{11.4}Si_{1.6}$, Appl. Phys. Lett. 78 (2001) 3675.
[56] J. Liu, M. Krautz, K. Skokov, T.G. Woodcock, O. Gutfleisch, Systematic study of the microstructure, entropy change and adiabatic temperature change in optimized La–Fe–Si alloys, Acta Mater 59 (2011) 2602.
[57] S. Talakesh, Z. Nourbakhsh, The density functional study of structural, electronic, magnetic and thermodynamic properties of XFeSi (X = Gd, Tb, La) and GdRuSi compounds, J Supercond. Nov. Magn. 30 (2017) 2143.
[58] A. Waske, E. Lovell, A. Funk, K. Sellschopp, A. Rack, L. Giebeler, P.F. Gostin, S. Fähler, L.F. Cohen, The impact of surface morphology on the magnetovolume transition in magnetocaloric $LaFe_{11.8}Si_{1.2}$, APL Mater 4 (2016) 106101.
[59] O. Perevertov, R. Schäfer, Influence of applied compressive stress on the hysteresis curves and magnetic domain structure of grain-oriented transverse Fe–3%Si steel, J. Phys. D: Appl. Phys. 45 (2012) 135001.